Piotr WIĘCEK [1], Bogusław WIĘCEK [2]
[1] LODZ UNIVERSITY OF TECHNOLOGY, INSTITUTE OF APPLIED COMPUTER SCIENCE, Stefanowskiego 18/22, 90-537 Łódź, Poland
[2] LODZ UNIVERSITY OF TECHNOLOGY, INSTITUTE OF ELECTRONICS, Wólczańska 211/215, 90 924 Łódź, Poland

Performance analysis of dual-band microbolometer camera for industrial gases detection

Abstract

In this paper we present a simplified performance analysis of wide-band microbolometer cameras for gas detection. The spectral characteristics of camera's elements such as detector, lens and filter were considered in this analysis. The parasitic radiation of IR filter that diminishes the contrast was included in the model. The exemplary results are presented for methane detection both in MWIR and LWIR bands of absorption.

Keywords: wide-band microbolometer detector, IR spectral transmission and absorption, configuration factors, IR absorption of methane.

Symbols:
α_d – absorption coefficient of the detector
α_λ – absorption coefficient of the detector
σ_λ – attenuation cross section in Beer-Lambert law
λ – wavelength
τ_f – transmission coefficient of IR filter
τ_λ – transmission coefficient of gas atmosphere
$F_{d\text{-}l}$ – radiation heat transfer configuration factor detector-filter
S_d – surface of the single-pixel detector
S_f – surface of IR filter
h – distance between filter and detector
r – radius of IR window/filter
f – focal distance of IR lens
F – F-number of IR objective
d – distance between the detector and mirror (~2.5 μm)
c, $c_i=n_i/V$ – gas concentration as number of molecules of a gas per volume unit, $1/m^3$
d_i – thickness of gas atmosphere, m
$e_{\lambda.T,f}$ – spectral exitance of IR filter, W/m^3
$e^{irr}_{\lambda.T,f}$ – spectral irradiance of the detector by IR filter, W/m^3
$e_{\lambda.,T,bb}$ – spectral exitance of the black body, W/m^3
$e_{\lambda,bb,gas}$ – spectral exitance of the black body passing the gas atmosphere, W/m^3
$E_{T,gas}$ – total radiation flux reaching the detector surface transmitted through gas and optics of a camera, W/m^2
E_T – total radiation flux reaching the detector surface transmitted through optics of a camera, W/m^2
cnt – contrast of IR signal for gas monitoring

1. Introduction

Nowadays, infrared imaging systems are more and more used for gas detection in industrial conditions. There are available photon, cooled infrared (IR) systems equipped with band-pass IR filters for gas detection [10, 11, 12, 13]. Such high sensitive portable IR cameras are cooperating with dedicated in-built software for gas leakage monitoring. Due to the cooling system of the detector they are heavy with limited time of battery continuous operation.

There are also cooled systems with tunable IR filtering using diffractive or interferometer filters mounted in front of the standard IR camera [13]. These filters allow IR spectrum analysis both in MWIR and LWIR with high spectral resolution.

Cooled IR cameras are still considered as portable systems, but in many applications they are unable to be used as a handheld apparatus, due to the high weight and power consumption. On the other hand in many cases, the main limit of practical usage of such systems is their high cost.

High sensitive uncooled IR systems became an alternative solution for spectrometric applications, especially for gas detection in polluted and explosive atmospheres [4, 9, 15, 16]. In contrast to cooled systems, uncooled cameras are low-cost, compact, portable, with long battery operation time [6, 7].

There is lack of literature showing the quantitative analysis of uncooled IR systems for spectrometric applications. This paper offers a simplified analysis of such systems, based on theoretical assumptions. It exhibits the main relations between the achievable contrast and main parameters of IR uncooled camera dedicated for gas detection.

2. A simplified model of optical path in microbolometer camera

The scheme of optical path for a single-pixel in a microbolometer focal plane array is presented in Fig. 1. One should notice that an IR filter is located in between lens and a detector. Typically, the filter is close to the detector window. We try to explain why it is not a recommended configuration.

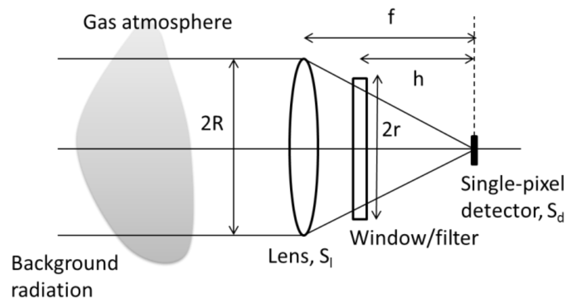

Fig. 1. Single-pixel optical path in a microbolometer detector

The microbolometer detector is made as a semiconductor membrane hanging above the IR mirror at the distance of one quarter of the middle wavelength of camera absorption band. For LWIR cameras it is about d=2.5 μm.

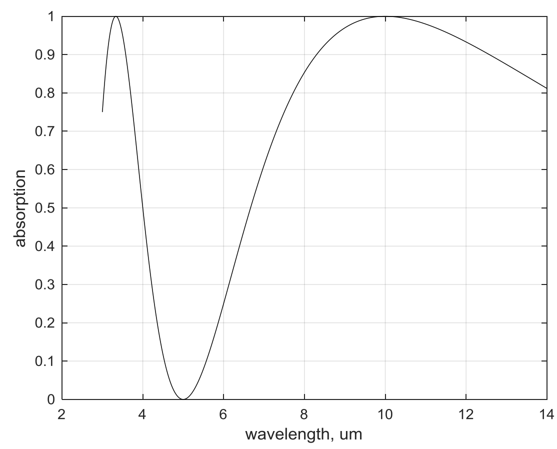

Fig. 2. Theoretical absorption characteristics of a microbolometer detector [4]

Such optical cavity augments the camera sensitivity for about 10 μm wavelength range, but on the other hand due to the optical interference it reduces the signal for half wavelength bandwidth, as shown in Fig. 2 [4].

Taking into account interference of incident and reflected radiation, the absorption coefficient of the detector α_d can be approximated as:

$$\alpha_d = \left[\sin\left(\frac{2\pi}{\lambda}d\right)\right]^2 \qquad (1)$$

The wide-band microbolometer detector acts as a dual-band device having 2 maximal points of the spectral absorption characteristic near 3 and 10 μm wavelength. Such spectral selective characteristics can be enhanced by addition filters.

There are available IR filters and windows that can be used for dual band microbolometer cameras [4, 6, 18]. Due to the spectral characteristics of detector's absorption, it seems to be reasonable to use wide band-pass IR window instead of narrow single-wavelength filters. The exemplary characteristic of a commercially available window made of Ca_2F is presented in Fig. 3.

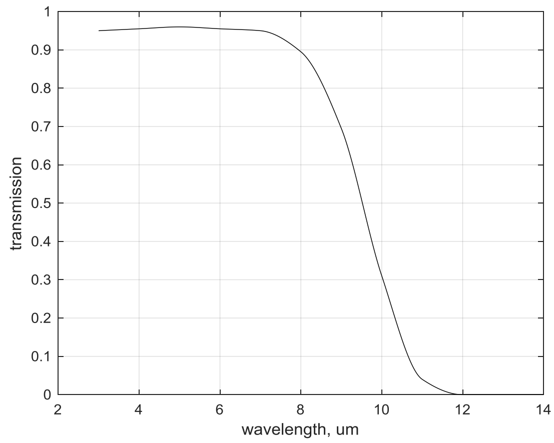

Fig. 3. Approximated characteristic of IR Ca_2F window [18]

Combining the characteristics from Figs. 2 and 3, the relative spectral attenuation of the signal reaching the detector is shown in Fig. 4.

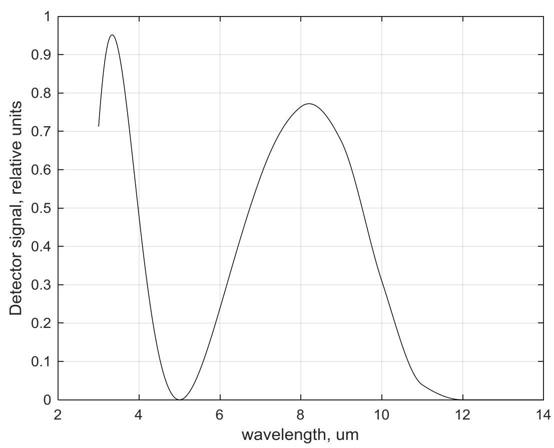

Fig. 4. Combined dual-band characteristic of broad-band IR detector (from Fig, 2 and 3)

In addition, the attenuation of lens mainly depends on the objective aperture number F [7,8]. As typically F =1 for microbolometer cameras, the transmission through lens is no greater then 20%.

Finally, one can conclude that the overall attenuation of the black body radiation at the detector surface can be expressed as:

$$\tau_{\lambda,cam} = \frac{1}{4F+1}\alpha_d \cdot \tau_f \qquad (2)$$

Let's now analyze the parasitic radiation of a filter that can affect contrast of images while detecting gases. Assuming that the filter is between lens and detector, the analysis is based on mutual radiation heat exchange [1, 5, 8]. According this theory, the amount of energy falling on a detector depends on the radiation heat transfer configuration factor between the surfaces of filter and detector, and can be expressed as:

$$e_{\lambda,T,f} = e_{\lambda,T,bb}(1-\tau_f)F_{d-l}\frac{S_d}{S_f} \qquad (3)$$

where the configuration factor detector-lens F_{d-l} can be calculated using eq. (4) [8]:

$$F_{d-l} = \frac{1}{\left(\frac{h}{r}\right)^2+1} \qquad (4)$$

Due to the low values of emissivity and configuration factor, the radiation energy of the filter is relatively low in contrast to the blackbody radiation in the same temperature. Fig. 5 shows the spectral exitance generated by the filter with the spectral characteristic shown in Fig. 3.

A comment is needed concerning eqn. (3). This formula presents the radiation approaching the detector in reference to the surface of the emission surface. Many authors use irradiance to describe the radiation energy referred to the surface of the detector. Irradiance can be easily obtained from eqn. (3) as:

$$e^{irr}{}_{\lambda,T,f} = e_{\lambda,T,f}\frac{S_f}{S_d} \qquad (5)$$

One can notice that irradiance of the detector is substantially higher then exitance given by eq. (3), but both formulae present the same amount of radiation power falling on the detector's surface.

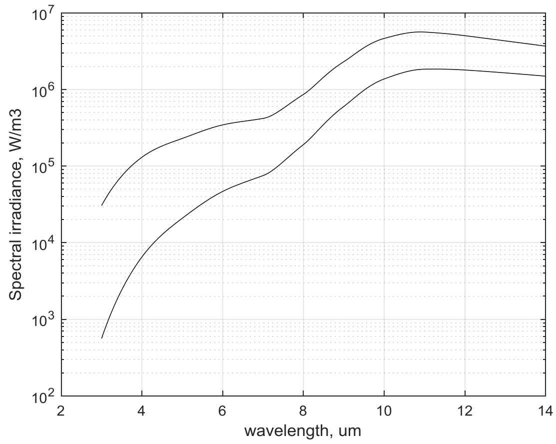

Fig. 5. Filter spectral irradiance of a detector surface for 2 values of filter temperature, T=300 K (lower) and 400 K (upper)

The gas attenuates the IR radiation passing through. This attenuation is very dependent on wavelength for a given gas, its concentration and thickness of gas atmosphere.

Using Beer-Lambert law, one can derive the transmission coefficient as a function of concentration c and thickness of gas atmosphere x [1,7].

$$\tau_{\lambda,gas}(x) = e^{-\sigma_\lambda c x} \qquad (6)$$

In consequence, if we know the concentration of the gas and the thickness of gas atmosphere, it is possible to recalculate the transmission coefficient for required environmental conditions.

$$\tau_{\lambda,gas}(d_2,c_2) = \tau_{\lambda,gas}(d_1,c_1)^{\frac{c_2 d_2}{c_1 d_1}} \qquad (7)$$

There are available models and spectral characteristics of transmission of different gases and their mixtures [2, 17]. The exemplary low-resolution curves of spectral transmission through methane atmosphere are presented in Figs. 6 and 7.

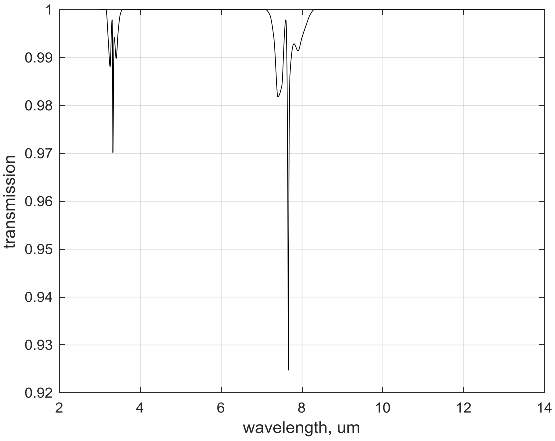

Fig. 6. Low resolution approximation of transmission for low concentration methane atmosphere of thickness d=1 mm

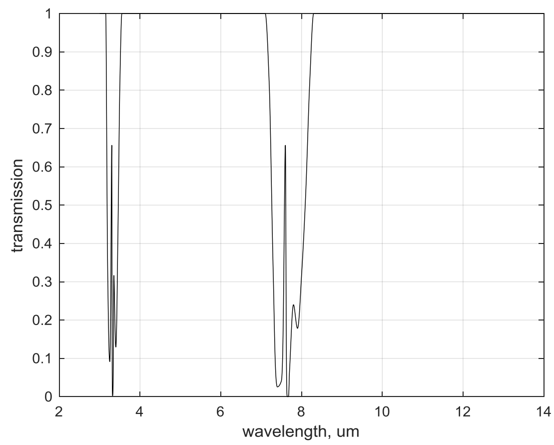

Fig. 7. Low resolution approximation of transmission for low concentration methane atmosphere of thickness d=0.2 m

It is worth to compare the amount of energy generated by an IR filter or window with energy reaching the detector originated from a black-body (background) and selectively filtered by a monitored gas.

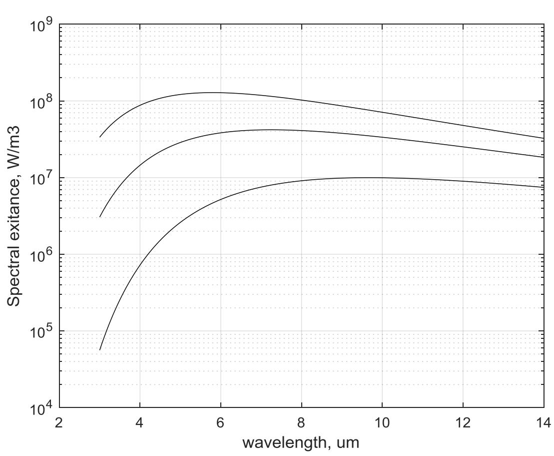

Fig. 8. Spectral exitance of a black body at temperature 300K (bottom), 400K (middle) and 500K (top)

As it is shown in Fig. 8, the energy emitted by the background depends on its temperature and it is much larger than the parasite radiation of the filter (Fig. 5). It can be concluded that for high temperature of background (T>500 K), the energy in MWIR band is larger than in LWIR spectral range. It can have an influence of the total sensitivity and thermal contrast of wide-band microbolometer cameras.

3. Simulation results

Using the model presented above, couple of simulations have been performed. In order to estimate the performance of uncooled wide-band IR system, the radiation signal's contrast was defined, as in eqn. (8).

$$\boldsymbol{cnt} = \frac{E_T - E_{T,gas}}{E_T}\,\mathbf{100}\% \tag{8}$$

where:

$$\mathrm{E_T} = \int_{\lambda_1}^{\lambda_2} e_{\lambda,T,bb}\,\tau_{\lambda,cam} d\lambda + \int_{\lambda_1}^{\lambda_2} e^{irr}{}_{\lambda,f}\, d\lambda \tag{9}$$

$$\mathrm{E_{T,gas}} = \int_{\lambda_1}^{\lambda_2} e_{\lambda,T,bb}\,\tau_{\lambda,cam}\tau_{\lambda,gas} d\lambda + \int_{\lambda_1}^{\lambda_2} e^{irr}{}_{\lambda,f}\, d\lambda \tag{10}$$

The IR filter of the same diameter as the lens was mounted in between lens and a detector, close to lens in the camera (Fig. 1). For the simulation presented in this research, a MATLAB program was developed. The IR objective with F=1 was selected. The simulations were performed for 17 μm IR VOx detector and 2r=3 cm lens diameter. Chosen results are presented in Tables 1–4.

Tab. 1. Total radiation power at the surface of detector and the contrast for different background temperature for methane detection, λ = (3-14) μm, atmosphere thickness d=0.2 m, methane concentration c ≈ 10N_A/m^3 in normal conditions, with IR filter, filter temperature 300 K

Background radiation temperature, K	Total background radiation, E_T, W/m^2	Total radiation through methane, $E_{T,gas}$, W/m^2	Signal's contrast, *cnt*, %
300	19.22	16.91	11.99
400	63.09	51,47	18.42
500	168.78	134.71	20.18

Tab. 2. Total radiation power at the surface of detector and the contrast versus thickness of methane atmosphere, λ = (3-14) μm, for background temperature T = 400 K, methane concentration c ≈ 10N_A/m^3 in normal conditions, with IR filter, filter temperature 300 K

Thickness of methane atmosphere, m	Total background radiation, E_T, W/m^2	Total radiation through methane, $E_{T,gas}$, W/m^2	Signal's contrast, *cnt*, %
0.001	63.09	62.94	0.24
0,01	63.09	61.65	2.28
0.1	63.09	54.68	13.32

Tab. 3. Total radiation power at the surface of detector and the contrast versus thickness of methane atmosphere, λ = (3-14) μm, for background temperature T = 400 K, methane concentration c ≈ 10N_A/m^3 in normal conditions, no IR filter

Thickness of methane atmosphere, m	Total background radiation, E_T, W/m^2	Total radiation through methane, $E_{T,gas}$, W/m^2	Signal's contrast, *cnt*, %
0.001	114.25	114.08	0.15
0,01	114.25	112.69	1.36
0.1	114.25	105.11	7.99

Tab. 4. Total radiation power at the surface of detector and contrast versus thickness of methane atmosphere, λ = (7-14) μm, for background temperature T = 400 K, methane concentration c ≈ $10N_A/m^3$ in normal conditions, with IR filter, filter temperature 300 K

Thickness of methane atmosphere, m	Total background radiation, E_T, W/m^2	Total radiation through methane, $E_{T,gas}$, W/m^2	Signal's contrast, *cnt*, %
0.001	48.46	48.31	0.31
0,01	48.46	47.09	2.83
0.1	48.46	40.51	16.41

Analyzing the data in the presented Tables 1-4, the general conclusions can be drawn. First, as it is expected the contrast depends on thickness of the methane atmosphere. Thickness of a few cm is enough to detect the gas. IR radiation energy depends on the width of absorption wavelength range. The higher radiation signal for wide-band detector confirms the better detection of gas due to the limited NETD and higher noise level of microbolometer cameras in contrast to photon, cooled ones.

4. Dual-band IR microbolometer camera for gas detection

Recently, the wide-band camera based with 640×480 VOx high-sensitive, 17 μm pitch detector, has been developed [15, 16] – Fig. 9. This system is equipped with the wheel for the shutter and 2 additional IR filters. Dedicated software for real-time gas detection has been developed in Java environment [4].

Fig. 9. Wide-band 3-14 μm IR camera for gas detection [16]

Implemented image processing algorithms operates on the movement detection basis. It allows overlapping gas signatures with the original image as it is shown in Fig. 10.

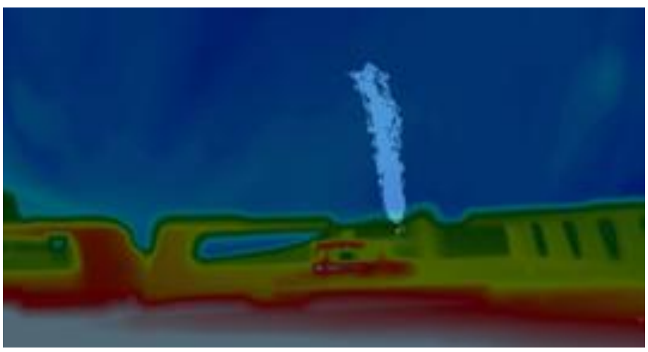

Fig. 10. Natural gas detection using wide-band (3-14) μm IR camera [16]

5. Conclusions

In this research we have developed the radiation model of the optical path in the wide-band microbolometer camera. The results confirm the higher radiation intensity for wide-band systems in comparison to LWIR cameras. It results in higher sensitivity of the wide-band IR systems; however the contrast between sound and area with methane is slightly lower. Spectral filtering enhances the radiation signal contrast of detected gases but it decreases the overall radiation reaching the detector. The filter can be mounted either between the lens and the detector or in front of the lens. In both configurations the filter should be placed as close to the lens as possible. Temperature of the filter has an impact of the sensitivity and contrast of the camera, but this analysis is not presented in details in this paper.

6. References

[1] Siegel R., Howell J.R.: Thermal Radiation Heat Transfer. 3rd ed., Taylor and Francis, Hemisphere Publishing Corporation, ISBN 0-89116-271-2, 1992.

[2] Rothman L. S., Jacquemart D., Barbe A., Chris Benner D., Birk M., Brown L.R, Carleer M.R., Chackerian C. Jr., Chance K., Coudert L.H., Dana V., Devi V. M., Flaud J.M., Gamache R.R., Goldman A., Hartmann J.M., Jucks K.W., Maki A. G., Mandin J.Y., Massie S. T., Orphal J., Perrin A., Rinslando C.P., Smito M. A. H., Tennyson J., Tolchenov R. N., Toth R. A., Vander Auwera J., Varanasi P., Wagner G.: The HITRAN 2004 molecular spectroscopic database. Journal of Quantitative Spectroscopy and Radiative Transfer, 96, (2005), pp. 139-204.

[3] Talghader J. J., Gawarikar A. S., Shea R. P.: Spectral selectivity in infrared thermal detection. Light: Science & Applications, 1, e24, 2012.

[4] Wiecek P.: A method for automatic gas detection using wide-band 3-14 μm bolometer camera, 14th Quantitative InfraRed Thermography Conference, Berlin 2018, http://qirt.org/archives/ qirt2018/papers/ p32.pdf.

[5] Sala A.: Radiacyjna wymiana ciepła. WNT, Warszawa 1982, (in Polish).

[6] Więcek B., Pacholski K., Olbrycht R., Strąkowski R., Kałuża M., Borecki M., Wittchen W.: Termografia i spektrometria w podczerwieni, Zastosowania przemysłowe, Warszawa 2017, (in Polish).

[7] Więcek B., De Mey G.: Termowizja w Podczerwieni podstawy i zastosowania PAK z Warszawa 2011, (in Polish).

[8] http://www.thermalradiation.net/indexCat.html.

[9] https://www.flir.com/news-center/press-releases/flir-launches-its-first-uncooled-methane-gas-detection-camera/.

[10] https://www.ulirvision.co.uk/gas-infrared-camera-ti330.html.

[11] https://www.flir.com/contentassets/ec52cc80e5d94f8fa3175ed1323bd10c/gas-detection-guidebook.pdf.

[12] http://www.flir.co.uk/uploadedFiles/Store/Products/OGI/GFx320/FLIR-GFx320-Datasheet-EN.pdf.

[13] https://www.telops.com/

[14] http://www.scd.co.il/Bird-640-17-Ceramic-Packaging.

[15] http://www.maxtor.net.pl/.

[16] http://www.texosystems.pl/.http://senseair.senseair.com/senseair/gases-applications/methane-ch4/.

[17] http://webbook.nist.gov/.

[18] https://www.thorlabs.com/newgrouppage9.cfm?objectgroup_id=3978

Received: 08.06.2018 Paper reviewed Accepted: 03.08.2018

Piotr WIĘCEK, MSc

He graduated from the Faculty of Electrical, Electronic, Computer and Control Engineering Lodz University of Technology in 2011. Actually, he is the PhD student of the computer science. NIR and IR thermography, image processing and deep learning systems are his areas of research. Actually, he works as a software developer for Java, C and C# object-oriented applications. He is co-author 6 JCR publications on NIR systems and 3D image reconstruction for textile research applications.

e-mail: pwiecek@gmail.com

Prof. Bogusław WIĘCEK

Prof. Bogusław Więcek is the head of the Electronic Circuits and Thermography Department at the Institute of Electronics, Lodz University of Technology. He specializes in computer thermography and modelling thermal effects in electronic devices and circuits. He is a member of the scientific committee of the international Quantitative Infrared Thermography Conference and the chairmen of the Thermography and Thermometry in Infrared Conference.

e-mail: boguslaw.wiecek@p.lodz.pl